

# Shear-Wave Radiation Patterns from Explosive and Earthquake Sources in Scattering, Heterogeneous Media

Peter Nelson (D \*1, Neala Creasy (D1

<sup>1</sup>Earth and Environmental Sciences Group, Los Alamos National Laboratory, Los Alamos, USA

Author contributions: Conceptualization: PN, NC. Data Curation: PN. Formal Analysis: PN, NC. Funding Acquisition: PN, NC. Investigation: PN, NC. Methodology: PN, NC. Project Administration: PN, NC. Resources: PN, NC. Software: PN, NC. Supervision: PN, NC. Validation: PN, NC. Visualization: NC. Writing – original draft: PN, NC. Writing – review & editing: PN, NC.

**Abstract** Distinguishing whether a seismic event is an earthquake or an explosion is a core problem in explosion monitoring. For simplistic models, earthquakes produce a predictable S-wavefield based on their radiation pattern, while an explosion produces no S-wavefield. However, observations from nuclear tests show that explosions can produce significant S-wave energy on both horizontal components. We perform numerical experiments using SPECFEM to constrain when an S-wavefield generated from an explosion might differ from one produced by an earthquake. We generate the S-wavefield for our explosions by placing the source location within a small region consisting of large velocity heterogeneities. For the 2D cases investigated here, a crucial condition is that the size of the region of heterogeneities must be much smaller (approximately 1/12th) than the minimum wavelength of the wavefield for our simulation setups. We investigate both isotropic heterogeneities and anisotropic heterogeneities. Initial results demonstrate that the heterogeneous region lowers the P/S amplitude ratios of an explosion. The presence of strong anisotropic heterogeneities near the source can also produce an S-wavefield with similar amplitudes to the P-wavefield. Lastly, we show that S-wave polarization angles vary as a function of azimuth and distance for explosive sources in the presence of small-scale heterogeneities.

**Non-technical summary** Earthquakes and explosions can appear similar when recorded on seismometers. Distinguishing between these events is a core problem in explosion monitoring. In an idealized Earth, earthquakes produce a predictable P- (primary) and S-wavefield (secondary wave produced by faulting). However, explosions are idealized to be pure outward forces, producing a strong P-wavefield and no S-wavefield. Yet, observations from nuclear tests have shown that explosions can produce significant S-wave energy. We perform 2D and 3D numerical experiments to better constrain the conditions in which an S-wavefield generated from an explosion might differ from one produced by an earthquake. We generate the S-wavefield for our explosions by placing the source within a small region with highly varying seismic velocities and densities (i.e., heterogeneity). For the 2D cases investigated here, a crucial condition is that the size of the heterogeneities must be much smaller than the minimum wavelength of the wavefield. We investigate the ratio between P and S-wavefields from our simulations, called P/S ratios. For explosions, this ratio decreases in the presence of these heterogeneities and can be similar in scale to P/S ratios of earthquakes. For earthquakes, the P/S ratio does not change as much.

Production Editor:
Gareth Funning
Handling Editor:
Paula Koelemeijer
Copy & Layout Editor:
Hannah F. Mark

Received: September 26, 2023 Accepted: October 3, 2025 Published: November 11, 2025

## 1 Introduction

Explosive sources have consistently produced shear waves that have large amplitudes on the transverse component (Blandford, 1981; Mykkeltveit and Husebye, 1981; Priestley et al., 1990). An explosive source, assuming it is pure and idealized with no deviatoric component, does not generate SH-waves (transverse component seismic energy) in an isotropic 1-D, layered velocity model. These idealized explosions contain energy only within the source-receiver plane. The only S-waves that are generated are from the conversion of P-waves due to scattering and discontinuities within the Earth. As a result, S-wave generation complicates the discrim-

ination of different source types, such as explosions, earthquakes, and cavity collapses (Taylor et al., 1989).

Distinguishing whether a recorded seismic event is an earthquake or explosion is a core problem in explosion monitoring (Nuttli, 1986; Patton, 1991; Richards and Zavales, 1990; Bowers and Selby, 2009; Coyne et al., 2012). A common approach is to analyze P-to-S amplitude and spectral ratios (Hartse et al., 1997; Xie and Patton, 1999; Jenkins and Sereno, 2001; Walter et al., 2018; O'Rourke et al., 2016; Houng, 2017; Wang et al., 2020). Theoretically, an explosion or meteoroid impact should produce a higher ratio of P-to-S energy (P/S ratios) than an earthquake; however, historical nuclear tests have shown that this is not always true (Press and Archambeau, 1962; Brune and Pomeroy, 1963; Aki et al., 1969;

<sup>\*</sup>Corresponding author: pln@lanl.gov

Priestley et al., 1990; Richards and Kim, 1997; Vavryčuk and Kim, 2014). For better accuracy, P/S measurements require path and attenuation corrections because P-and S-waves have different propagation paths through the Earth. Depending on the location, these corrections can be large and uncertain.

Several explosion experiments have been conducted over the years demonstrating how S-waves can be generated from explosions. At the Source Physics Experiment (SPE) at the Nevada National Security Site (NNSS) (Snelson et al., 2013), two explosions were set off in the same location, but the near-field seismic properties were different. SPE-2 was a 992-kg TNT -equivalent shot set off at 45 m depth. SPE-3 (an 899-kg TNT-equivalent shot) followed SPE-2 and was placed in the same location as SPE-2. The SPE-2 and SPE-3 recordings show that the two shots produced almost identical wavefields (Mellors et al., 2012). This result suggests that either near-source heterogeneities do not influence the observed far-field in the real Earth or SPE-2 did not damage the rock enough to significantly impact its near-source small-scale heterogeneities.

Another experiment, where two explosions were set off in the same location, was the Salmon and Sterling nuclear tests, conducted in the 1960s. Salmon (5.3 kiloton) and Sterling (0.38 kiloton) were a pair of tests designed to study the effect of having a nuclear explosion decoupled from the surrounding salt formation. The first explosion, Salmon, was designed to excavate a cavity in a salt formation in which Sterling was detonated (Healy et al., 1971). Salmon created an approximately 17 m diameter spherical cavity that had a flat bottom from molten salt recrystallizing (Xu et al., 2009). The explosion also damaged the salt up to 60 m away from the detonation point (Denny and Goodman, 1990). Salmon did not produce any observable S-waves in the near-field while Sterling did (Perret, 1968). All other known decoupled explosions have produced shear waves (Xu et al., 2009). Xu et al. (2009) modeled the Sterling explosion and found that with an aspherical salt cavity geometry, they were able to reproduce the observed near-field S-

Another experiment tested slightly different source locations so that the far-field propagation was similar to each test, but the specific source area was different. In the New England damage experiment (NEDE), charges of different chemical compounds were set within tens of meters of each other and were recorded 5-30 km away. All NEDE explosions produced Love waves. Shots 1 and 2 produced similar Love waves, but the Love waves from the other three shots are unique (Stroujkova et al., 2012).

As a result, many studies and experiments have demonstrated that S-waves can be generated from an explosive source, especially by near-source small-scale heterogeneities (Leavy, 1993; Burgos et al., 2016), anisotropy (Mandal and Toksöz, 1990), tectonic release (Aki et al., 1969; Ekström and Richards, 1994), emplacement conditions, activation of nearby faults, a non-uniform in situ stress (Vorobiev, 2022), path effects (Gupta et al., 1992; Myers et al., 1999; Rodgers et al., 2010). There is significant geologic and seismic evidence for small-scale scatterers within Earth's

crust (Singh and Herrmann, 1983). Small-scale heterogeneities can influence the seismic wave field, such as amplitudes, travel-times, spectra, coda (e.g., Sato et al., 2012), and excitation of secondary microseism Love waves (Gualtieri et al., 2019). Significant work has been conducted on how small-scale heterogeneities influence the global wavefield in both the near- (Hirakawa et al., 2016) and far-field (Leng et al., 2020; Pienkowska et al., 2020).

As Leavy (1993) described, when scattering occurs within a single wavelength near the seismic source, the dominant scattered wave is of the quadrantal type, where the frequency dependence is determined by the source frequency. Quadrantal type is when the wavefield has a pattern where there are two symmetry axes 90 degrees apart, thus creating four equal quadrants. Earthquake sources produce a predictable pattern of Swave polarization based on a moment tensor (Aki and Richards, 2002), which depends on the take-off angle (related to receiver-source distance and velocity model) and azimuth. S-wave polarization angle is defined as the orientation of the particle motion of the S-wave (which combines SH and SV energy). Figure 1 illustrates the polarization angle and normalized SH and SV wave amplitudes for three different types of earthquakes for an Swave recorded at an epicentral distance of 10° away as a function of azimuth. There is a clear and unique polarization angle pattern for each type of event which could be used to infer the source's radiation pattern. An explosion source in a 1D flat layer model will not produce any SH energy; therefore, any S-wave arrival will always have a polarization angle of zero (a pure SV wave). However, S-wave energy has been observed to be present on both the radial and transverse components, indicating strong SH energy (Richards and Kim, 1997).

In this article, we explore a relationship that has not been thoroughly studied - how the radiation pattern and polarization angles of an S-wave generated from an explosion change as a function of azimuth at regional distances. The advantage of using polarization angles over P/S ratios is that path corrections are not needed for a weakly anisotropic medium like the crust and upper mantle. This is because SH and SV waves generated from the same source should have nearly identical paths and attenuation. Building upon the results from Burgos et al. (2016), we explore how small-scale heterogeneities in the source region affect P/S ratios as a function of azimuth. We also explore which conditions must be satisfied to produce an S-wavefield. This study focuses on the generation of S-waves from an explosion in a 2D and 3D homogeneous medium with smallscale scatters that are either isotropic or anisotropic. We demonstrate for our simulation setups that an explosive source will produce S-waves with amplitudes comparable to the P-wavefield when the region of heterogeneities is at least 1/12 the size of the S-wave wavelength and is extremely close to the source (within 100-200 m). We also demonstrate how the S-wavefield changes with different source frequency, heterogeneity length scale, and type of small-scale heterogeneities (isotropic and anisotropic) for both an explosive and earthquake source.

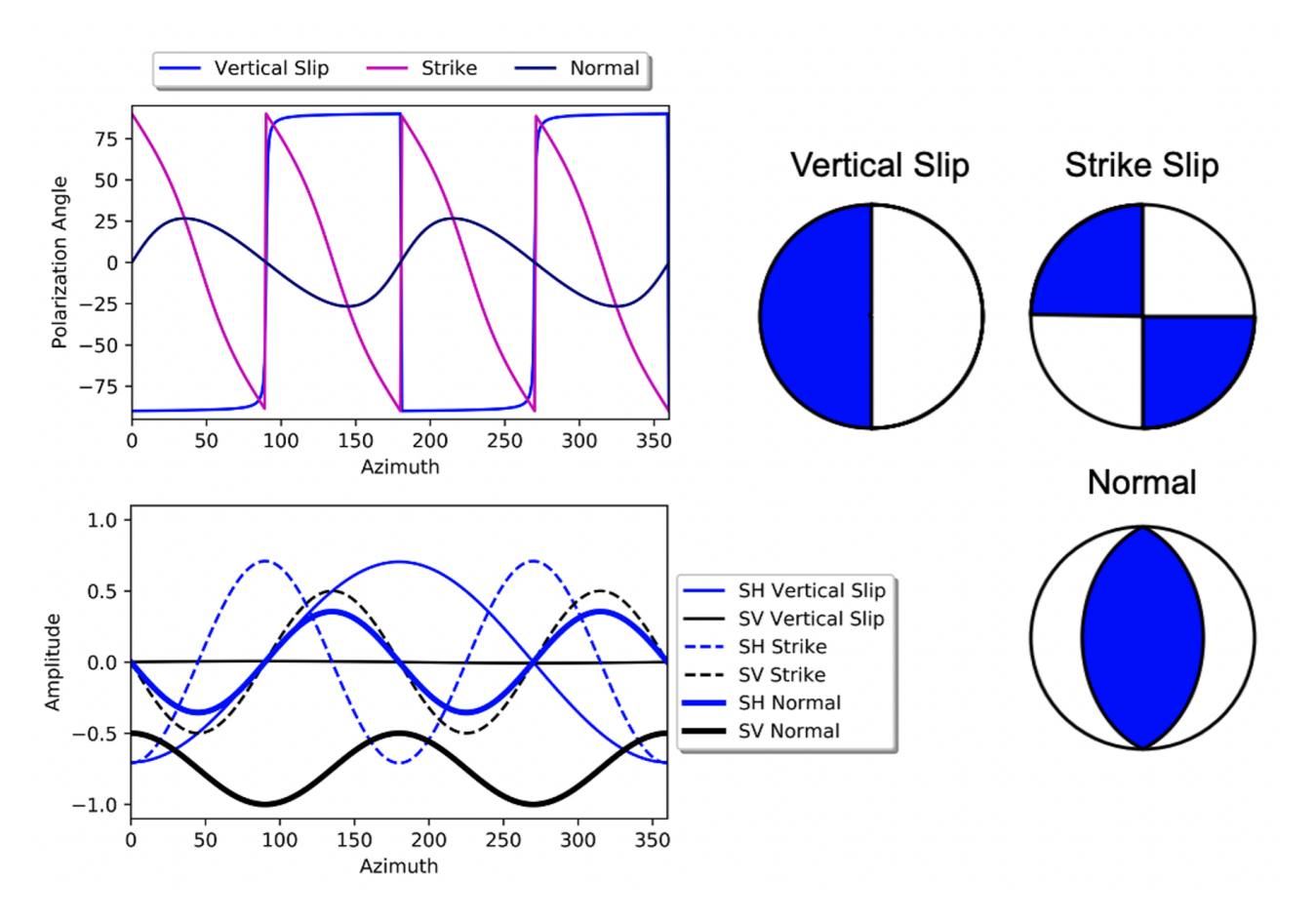


**Figure 1** Calculated shear-wave normalized amplitudes (bottom) and polarization directions (top) versus azimuth from the event for an S-wave at a distance of 10° that has a take-off angle of ~45° from the vertical for 1D global PREM. Normalized amplitudes are calculated based on Aki and Richards (2002) equations 4.89-4.91, which are dependent on the strike, dip, rake of the fault slip, take-off angle, source-receiver azimuth with the assumption that the ray is in the far field. Polarization angle is the arctangent of the SH and SV amplitudes (i.e., a polarization angle of 0° is a purely SV wave, while a polarization angle of  $\pm 90^\circ$  is a purely SH wave). Corresponding double-couple focal mechanisms are displayed to represent the major source types (vertical dip-slip, strike slip, and a normal fault, dipping at  $\pm 45^\circ$ ) used in the subplots on the left. Azimuth of zero degrees is pointing upward or north relative to the beach balls.

### 2 Numerical Methods

To simulate our wavefield for the 2D cases, we use the spectral element method-based wave propagation solver SPECFEM2D (Komatitsch and Vilotte, 1998; Tromp et al., 2008; Peter et al., 2011). SPECFEM2D is capable of both isotropic and anisotropic wave propagation in 2D and of handling high frequency (~8 Hz) wavefield simulations in small model domains without the need for high performance computing.

Figure 2 demonstrates the model setup for the 2D simulations. Our source (orange cross) is at the center of the domain with stations (green triangles) 25 km away from the source at 5° azimuthal increments. The domain is a homogeneous 100 by 100 km square with perfectly matched layer boundary conditions on all sides (Xie et al., 2014; Komatitsch and Tromp, 2002a). All simulations were conducted with a uniform grid with element size of 200 meters with 9 GLL points per element except for simulations where we did a mesh convergence test to explore the mesh size effect on the wavefield (Supporting Figure S3). We parameterized the

model by Vp, Vs, and density. The background material consists of approximate upper mantle properties with a Vp of 7.783 km/s, Vs of 4.500 km/s, and density of 3260 kg/m3. We chose mantle values as opposed to crustal values because the higher velocities are computationally cheaper for the high frequencies we simulate. These values correspond to a minimum S wavelength of ~560 m for 8 Hz and 9 km for 0.5 Hz, which is ~ 5 times larger than the element spacing. For the explosive sources, we applied a Gaussian source time function with a dominant frequency of 1 Hz and  $M_{xx} = M_{zz} =$  $10^{18}$  Nm and  $M_{xz}$  = 0, while for earthquakes we use  $M_{xx}$  =  $M_{zz}$  = 0 and  $M_{xz}$  =  $10^{18}$  Nm (strike slip). We selected a strike slip for comparison because it has the most varied azimuthal pattern. We placed the source at the center of the anomalous region to maximize the S-wave energy produced (see Burgos et al., 2016). The vertical direction in Figure 2 is the Z direction (up-down), and the horizontal direction is the X direction (left-right). Therefore, the radial component is calculated by rotating the seismograms, so the seismograms are oriented towards the source (parallel to the back azimuth), and the "trans-

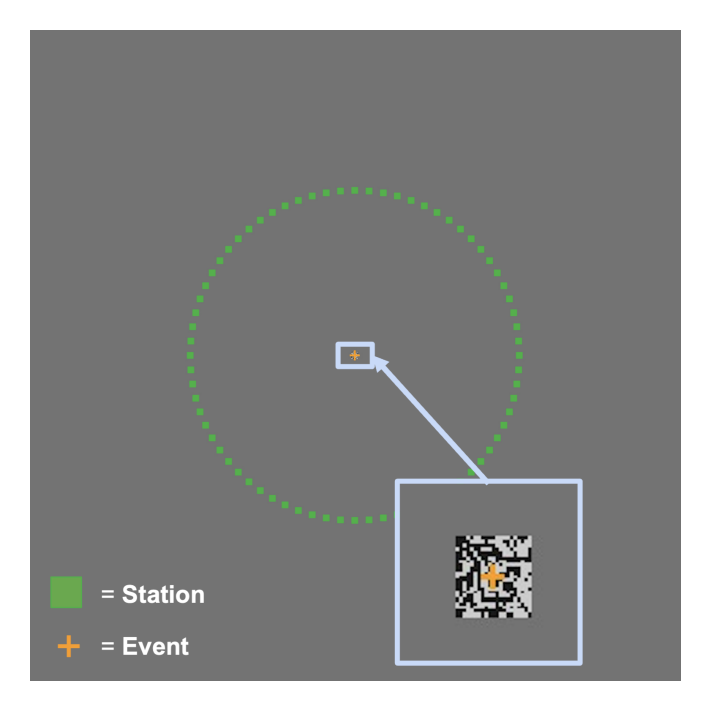


**Figure 2** Geometry of the seismic source/event (orange cross), stations/receivers (green squares), and an example of small-scale heterogeneities (entire region is 1 km) surrounding the source. The domain size is 100 by 100 km. Stations are 25 km away from the source. Colors (black and light gray) represent seismic velocity and density variations of  $\pm 25\%$  at each GLL point. Each point is randomly assigned a  $\pm 25\%$  or  $\pm 25\%$  variation from the background model.

verse" component is perpendicular to the back azimuth. We did not include any intrinsic attenuation in our calculations.

We also performed similar simulations in 3D using SPECFEM3D\_GLOBE (Tromp et al., 2008). For these calculations, we placed the source at the free surface with stations in a circle 400 km away from the source with the 1D AK135 model (Kennett et al., 1995). Moving to 3D simulations is crucial because the third horizontal component is absent in 2D simulations. Our model domain is 9° x 9° (~1000 km by 1000 km) with 768 elements in each direction and a depth of 220 km. The model has an average element size of 1.3 km. Ellipticity, topography, rotation, gravity, and attenuation are excluded in the calculations. For the earthquake source, we use  $M_{rt} = M_{rp} = 10^{25}$  dyne-cm (10<sup>18</sup> Nm) while all other components are zero. For the explosive source, each trace element in the moment tensor equals 10<sup>25</sup> dyne-cm (10<sup>18</sup> Nm). Lastly, the source time function is Gaussian with a half duration of 1 sec. To measure the Swave polarization in subsequent sections, we calculate the 2D PCA (Principal Component Analysis) for the windowed radial and transverse components, following the approaches of other studies (e.g., Li et al., 2021). All 2D synthetics are bandpass filtered from 0.14 Hz to 20 Hz, and 3D synthetics are filtered from 0.2 Hz to 1.5 Hz.

## 3 Results

## 3.1 S-wave Generation in 2D with Explosive Sources

We start by showing how small-scale heterogeneity near the epicenter of an explosive source can produce an S-wavefield, in agreement with the findings of Burgos et al. (2016). We placed a small region of smallscale isotropic heterogeneities in the middle of the simulation with a pattern that randomly assigns a value that is ± 25% Vp, Vs, and density relative to the background values to each GLL point (average GLL spacing is 50 m [1/90th of 1 Hz S-wavelength] with a minimum of 34.5 m). The heterogeneous region is centered on the source and is 1 km (2/9ths of the 1 Hz S-wavelength) across. This study also considers a Gaussian autocorrelation function (Sato et al., 2012) with a correlation length of 35 m and an RMS of 10% and 25%. Average RMS variations of crustal rock seismic velocities are typically ~10% based on geological surveys and welllog data (Sato, 2009) but can occasionally reach up to 25%. We did not explore other RMS variations as Burgos et al. (2016) explored this aspect extensively. Figure 3 shows the norm of displacement for a simulation with and without heterogeneity near the epicenter for an explosive and strike-slip source with a dominant source frequency of 1 Hz. The corresponding waveforms are shown in Figure S1 in the supporting information. Very similar modeling results were also found by Capdeville et al. (2010).

The length scale of the heterogeneous region is noticeably smaller than the 4.5 km wavelength of the Swave (for 1 Hz) in the background medium. For the homogenous simulation, a clear uniform P-wavefront radiates from the source as expected (Figure 3a). For the heterogeneous simulation, the P-wavefront now slightly varies with azimuth, but there also exists a large S-wavefront with a comparable amplitude to the Pwavefront (Figure 3b). A similar P and S-wave radiation pattern is produced with the Gaussian spectrum (Figure 3c-d), but the orientation of the S-wavefield changes, since the distribution of heterogeneities near the source varies with each new Gaussian spectrum that is generated. Additionally, the strength of the generated Swavefield relative to the P-wavefield decreases when RMS decreases. We also repeated the experiment with a double-couple earthquake source that has a moment tensor of  $M_{xx} = M_{zz} = 0$  and  $M_{xz} = 10^{18}$  Nm (Figure 3ef). With the addition of the heterogeneities near the source, the P-wavefield rather than the S-wavefield is most affected.

For an explosion to generate a strong S-wavefront, it is crucial for the epicenter to be located within the heterogeneity (Figure 4a). In Figures 4b-c, we move the source near the edge of the heterogeneous region in different locations. Both setups produce very weak S-waves compared to when the source is in the center. Figure 4d shows a case where the explosive source is located very close to the heterogeneity but not within it. As a result, only a weak S-wavefront forms.

In resulting figures, we measure P/S component en-

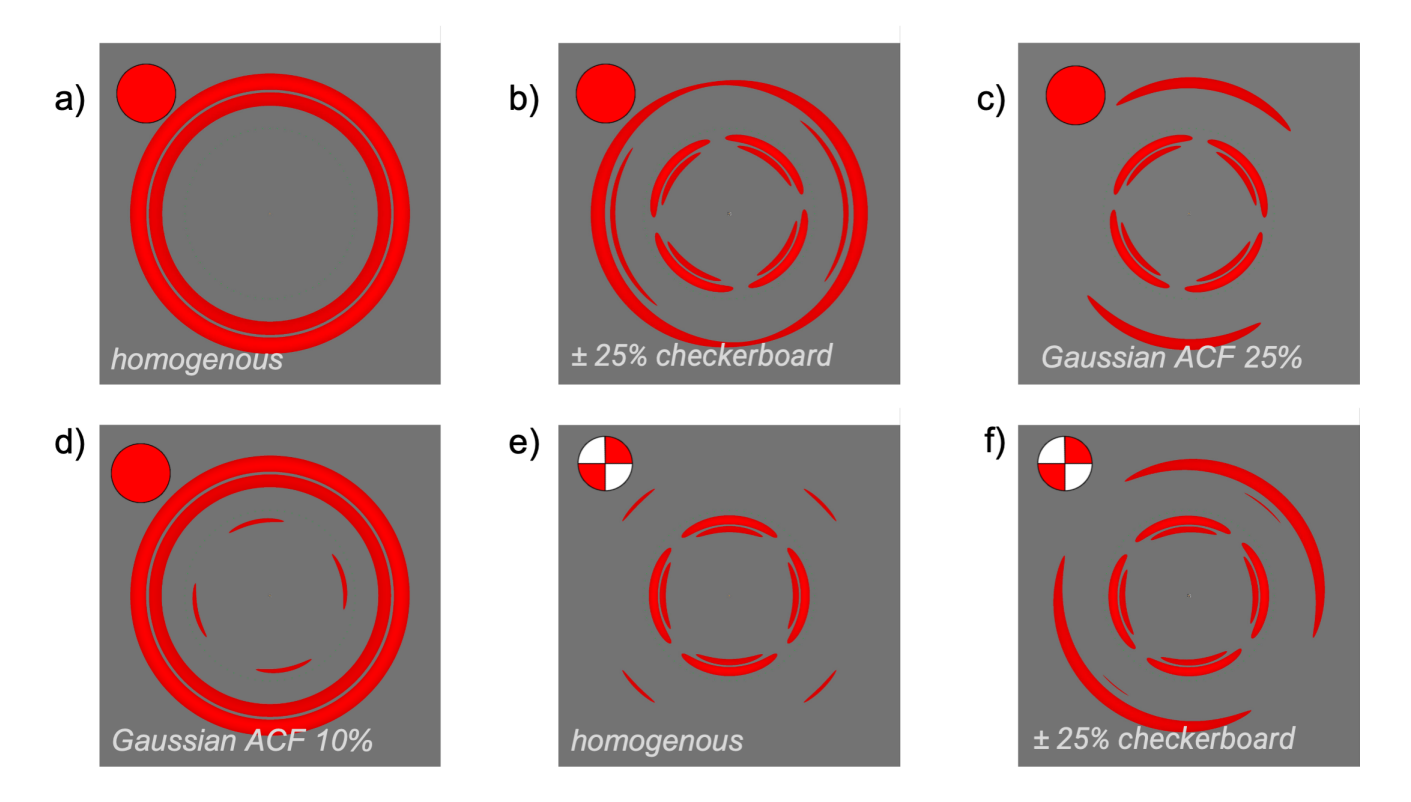


**Figure 3** Vertical 2D seismic displacement patterns of explosive (a-d) and strike-slip earthquake (e, f) events within a completely homogeneous medium (a, e). Beachballs represent the source type. In the first heterogeneous case (b, f), a 1 km region of randomized velocity and density heterogeneities of either positive 25% or negative 25% velocity and density variations are placed around the source, similar to a checkerboard. We also tested a Gaussian autocorrelation function (ACF) with an RMS of 25% (c) and 10% (d) and a correlation length of 35 m with an explosive source. The source and receiver geometry are that of Figure 2 and the dominant frequency of the source frequency is 1 Hz. The amplitudes in each wavefield snapshot and all subsequent snaps are displacement norm and amplitudes below 20% of the maximum amplitude are muted for figure clarity. See Figure S1 in supporting information for corresponding waveforms

ergy ratios (which is very similar to P/S amplitude ratios) to quantify the azimuthal strength of the S-wave field, using the following equation:

$$\frac{P}{S} = \sqrt{\frac{P_R^2 + P_T^2}{S_R^2 + S_T^2}} \tag{1}$$

The P/S ratio is the squared, summed energies of windowed P and S-wave component waveforms for each component (R = radial, T = transverse). Within this study, we do not apply corrections for Q because Q is constant in our simulations, and our sources are close to the receivers so that P and S-wave paths are similar. In 2D, we assume propagation in the horizontal directions only. Radial is the component pointing from the source to the receiver. The transverse component is orthogonal to the radial component (ZRT coordinates, but no Z component). An example of the summed energy for the P-wave for the radial component (R):

$$P_R = \frac{1}{N} \sum_{i=t1}^{i=t2} |d_i| \tag{2}$$

The energy is calculated for each waveform as the sum of the amplitudes d over the selected time window (series of indices i within the time window between indices t1 and t2) and then divided by the length of the window (N).

To validate that our simulations are accurate, we first compared our results to theoretical studies. The far field S-wave should result from the interaction between the source heterogeneities, specifically changes in rigidity or shear modulus (Supporting Figure S2), and the near-field evanescent part of the wavefield (see Aki and Richards 2002, p. 85, equation 4.35 or Leavy 1993). This near-field part of the wavefield is only important for distances that are a small fraction of the minimum wavelength and can be ignored at farther distances (Burgos et al., 2016). We show this by calculating P/S ratios for each waveform over the selected P- and Swaves with an explosive and earthquake source, where we only vary the Lamé parameters ( $\lambda$  and  $\mu$ ). When we only change  $\lambda$ , there is no change in P/S ratios compared to the homogeneous simulations, showing no S-wave field generated. However, when we changed  $\mu$ , the Swave field is generated in the explosive test case.

Additionally, we calculated a mesh convergence test to evaluate the simulation resolution to show that the S-wave fronts are not an artifact from coarse element spacing (Supporting Figure S3). In these tests, we use an explosive source with a dominant frequency of 1 Hz and a 1 km region of isotropic seismic heterogeneity. To make these tests as alike as possible given the different meshes, we alternate between positive (+25%) and negative (-25%) heterogeneities for Vp, Vs, and density from

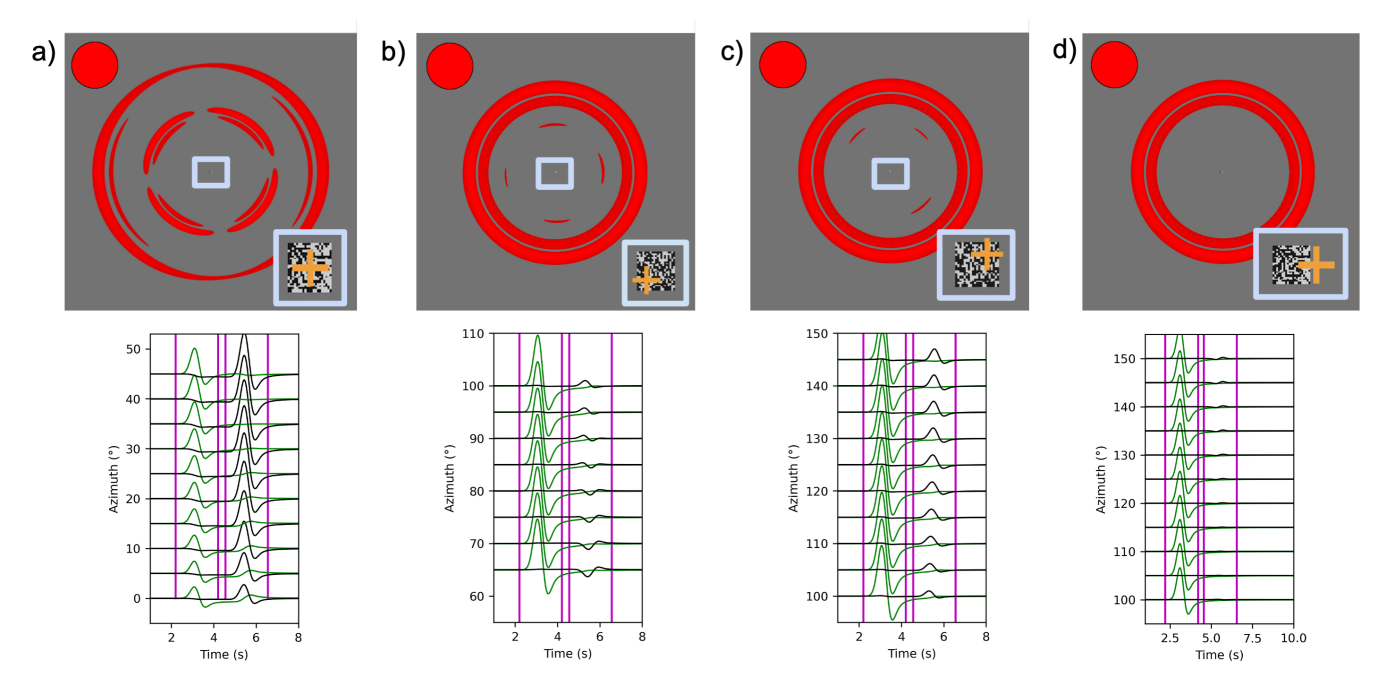


**Figure 4** 2D norm of displacement patterns and normalized seismograms (azimuths ~90°-180°) of explosive sources. An azimuth of 0° is up or North, where 90° is to the right or East. The source and receiver geometry are that of Figure 2 and the dominant frequency of the sources is 1 Hz. In the seismograms, vertical magenta lines are the window selections for P- and S-wave arrivals and the corresponding measurement windows for P/S ratios. Radial and transverse components are represented as green and black lines, respectively. (a) Displacement pattern and seismograms for when the explosive source is in the center of the region of heterogeneity. (b-c) The corresponding displacement patterns and seismograms for varying the source locations within the region of small-scale heterogeneities, shown within the insets. Some seismograms were amplified to see the S-wave clearer. (d) Displacement pattern and seismograms for when the explosive source is ~50 m from the region of heterogeneity.

the background values in four quadrants. As the mesh coarsens, the S-wave energy begins to decrease, especially with a 1000 m mesh. At an element size of 1000 m and 666 m, the minimum S-wave wavelength is ~3.4 and ~5 times the element size, respectively (minimum S-wavelength of 3.375 km for 1 Hz for the reduced velocity within the region of perturbations).

There is also a minimum threshold of the size of the region consisting of small-scale heterogeneities that is needed to generate an S-wavefield. Figure 5 illustrates a 1 Hz explosive source where the region of smallscale heterogeneities is changed in size (while maintaining the same length-scale of the small-scale heterogeneities) that alternate between positive (+25%) and negative (-25%) heterogeneities for Vp, Vs, and density from the background values, like a checkerboard. We vary the size of the region, using values of 100 m (1/45th), 250 m (1/18th), 350 m (~1/12th), 500 m (1/9th), 1 km (2/9th), 7.5 km (5/3rds), and 60 km (40/3rds). The values in parentheses correspond to the S-wavelength at 1 Hz relative to the element size. All simulations create an S-wavefield with an explosive source, but the amplitudes of the generated S-wavefield significantly reduces when the region size is less than 350 m (~1/12th). Furthermore, the relatively short-wavelength heterogeneities become invisible to the wavefront as it moves away from the source. For example, the P/S ratios for the 350 m and 60 km tests are nearly identical (Figure 5). Therefore, only the near-field heterogeneities influence the overall wavefield, while heterogeneities further away from the source (e.g., 60 km test) do not seem to change the P/S ratios at all. Lastly, there is a minimum distance that the heterogeneities need to be from the source to create a strong S-wave front.

In Figure 6, we completely enclose the source region by small-scale heterogeneities but keep the area near the source the same material as the background model. The spacing between the source and the inside edge of the heterogeneous region is 250m (1/18th). In Figure 6a, the dominant source frequency is 1 Hz, and we do not observe any S-wave caused by the heterogeneity. In Figure 6b, we change the dominant source frequency to 8 Hz (4/9th) and we see a scattered S-wavefront. The increased frequency of the source makes the Pwavelength comparable to the size of the heterogeneity; therefore, we observe a scattered S-wavefield. In comparison, when the source was at 1 Hz, the wavelength of the P-wavefield was too large to be sensitive to the heterogeneity around the source. In Figure 6c, we change the distance between the source and the inside edge from 350 m to 0 m and measure the P/S ratios as a function of azimuth for a 1 Hz source. Around 175-200 m ( $\sim$ 1/22 to  $\sim$ 1/25th), the P/S ratios start to decrease with decreasing source to heterogeneity distance, which indicates the distance when near source terms start to influence the wavefront for this given frequency.

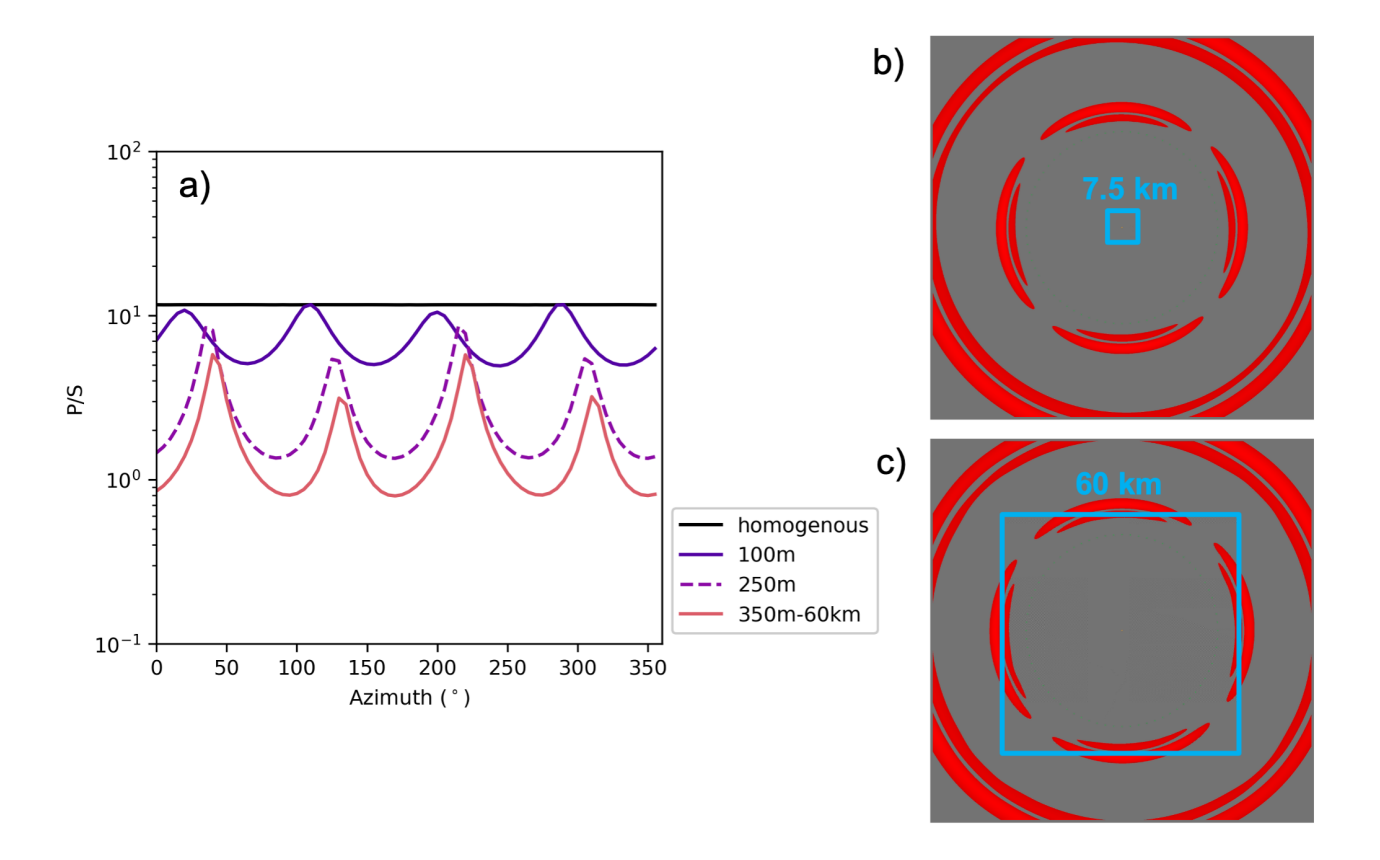


**Figure 5** (a) Windowed P/S ratios for 2D synthetic seismograms plotted as a function of azimuth from the source for different sized heterogeneous regions that surround an explosive source. The source is in the middle of the domain for each scenario. In all scenarios, there is a region of small-scale heterogeneities except for the homogeneous case (black line), but we vary the size of the region for each simulation (100 meters = dark purple, 250 m = dashed medium purple, 350 m - 60 km = solid orange). All simulations with regions greater than 350 m overlap. In all other simulations, we use the 1 km sized heterogenous region. We also use the 100 m mesh in each of these scenarios (see Figure S3). Waveform snapshots show the 2D displacement norm for two scenarios with a 7.5 km (b) and 60 km (c) boxed regions of heterogeneous material (outlined in blue) at 8 seconds.

#### 3.2 Source Frequency

Source frequency affects the P- and S-wave fields, as displayed in Figure 7. For this test, an explosion is placed within a 1 km region of small-scale heterogeneities, where the seismic parameters randomly vary by  $\pm 25\%$ in the Vp, Vs, and density relative to the background. We tested source frequencies of 0.5, 1, 2, 4, and 8 Hz. All source frequencies produced an S-wavefield with varying relative amplitudes. We also repeated this experiment using a 0.5 km region instead of 1 km. Each explosive case showed a similar azimuthal pattern of P/S ratios across all frequencies; however, the P/S ratios slightly decrease as frequency increases (see Supporting Figure S4). We observe a similar pattern when we use an earthquake source, where P/S ratios slightly decrease as source frequency increases. Figure 7b illustrates that as the source frequency increases, a coda is present after the S-wave arrival, which is another source of S-wave energy. We observe this coda for all 8 Hz simulations.

Overall, small-scale heterogeneities can lower the P/S ratios for all tested source frequencies for explosive sources, indicating that the source frequency is related to the generated S-wave energy and scale of heterogeneity. For earthquakes, P/S ratios modestly change de-

pending on the scale of the region of small-scale heterogeneities. For lower frequencies (such as 1 Hz) and larger regions of heterogeneity (relative wavelengths are between 1/4 to 1/5), P/S ratios of earthquakes and explosives are comparable. However, as source frequency increases and the region of heterogeneity decreases, the P/S ratios begin to differ. Lastly, the azimuthal pattern of P/S ratios for the strike-slip event depends on the source's radiation pattern. This azimuthal P/S ratio pattern would change with a different earthquake source. The maximum P/S ratio occurs when P has the largest amplitude in the radiation pattern, which can be seen in Figure 3e (P is maximum at 45°, 135°, 225°, and 315°).

# 3.3 The Influence of Anisotropic Heterogeneities on Radiation Patterns

Seismic anisotropy has also been demonstrated as a potential mechanism for S-wave generation from an explosive source (Martynov and Mikhailenko, 1984; Mandal and Toksöz, 1990; Maupin, 1990; Gajewski, 1993; Ben-Menahem and Sena, 1990; Ben-Menahem et al., 1991). Since we are mainly using 2D simulations, anisotropy in 2D is implemented into SPECFEM with the most general 2D case, where only the stress-strain relationship is calculated in the X and Z direction, requiring only 6 pa-

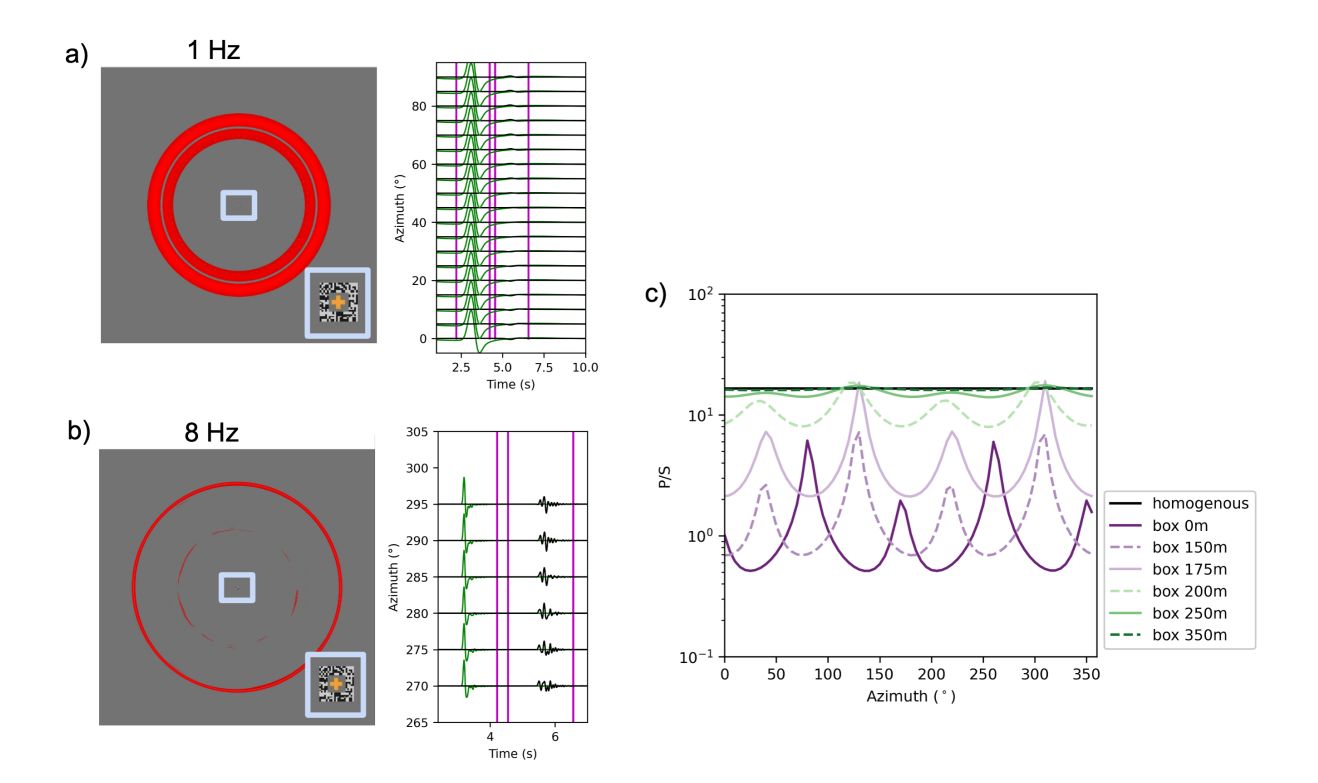


**Figure 6** 2D norm of displacement patterns and corresponding seismograms (azimuths ~0°-90°) of explosive sources with different source frequencies, (a) 1 Hz and (b) 8 Hz. The source and receiver geometry are that of Figure 2. In the seismograms, vertical magenta lines are the window selections for P and S wave arrival and the radial (green lines) and transverse components (black lines). The heterogeneous region is 1 km in size, but there is a smaller region of homogeneous background material that is 250 m across. (c) The corresponding P/S energy ratios for different sized boxes of homogeneous material within the heterogeneous region for 1 Hz source frequency. The 2D norm of displacement pattern for 250 m for a 1 Hz source is shown in (a).

rameters (C11, C13, C15, C33, C35, and C55 of the Voigt notation of the symmetric elastic tensor). We generated elastic tensors assuming a hexagonal symmetry using Anderson's parameters (Anderson, 1961) and the MSAT software (Walker and Wookey, 2012). These tensors are provided in Table S1 in the Supporting Information.

In Figure 8, we show that when the entire medium is anisotropic, S-waves are generated from both explosive and earthquake sources under a horizontal transverse isotropy (HTI) condition. Our results are nearly identical to previous numerical and analytical work (Ben-Menahem et al., 1991), as the explosion generates a significant amount of S-wave energy in the directions between axes of symmetry (see Figure 8a-b). One way to produce transverse component S-wave energy through anisotropy is akin to shear wave splitting of an SKS wave (Silver and Chan, 1991), where the radial SV energy of an SKS is split into radial and transverse component energy in the presence of anisotropy. In essence, anisotropy distorts radiation patterns and bends rays (Baker et al., 2012)

Figure 9 illustrates how small-scale anisotropic heterogeneities also produce an S-wavefield, comparable to the case with isotropic small-scale heterogeneities. In this test, the mesh elements alternate between the fast direction being horizontal and being vertical (similar to vertical and horizontal transverse isotropy – VTI and HTI, respectively), where the average isotropic vertical ending to the state of the state

locity is identical to the background medium. The anisotropic media are 20% anisotropic for P- and S-waves in both cases. For the earthquake source, adding anisotropic heterogeneities near the source does not significantly change the P/S ratios, while the isotropic small-scale heterogeneities have a stronger effect. In contrast, the explosive source produces P/S ratios that are more strongly influenced by isotropic heterogeneities than anisotropic ones.

Anisotropy is a 3D effect; therefore, to fully understand its effect on the explosive sources we need to expand our simulations to 3D. Maupin (1990) found that anisotropy can also split S-waves produced by explosions, such as the crustal phase Lg, but this effect has yet to be explored in a laterally varying 3D medium. Lg waves generated by explosions are typically dominated by SV energy; however, in the presence of crustal anisotropy, they may undergo shear wave splitting. Therefore, due to the presence of strong anisotropy that can be present in the deep crust and Earth's upper mantle (e.g., Brownlee et al., 2017; Moschetti et al., 2010; Savage, 1999), seismic anisotropy may influence energy partitioning for Pg and Lg generated from an explosion (e.g., Nelson et al., 2023). Anisotropic 3D simulations are beyond the scope of this study but are a promising future research direction.

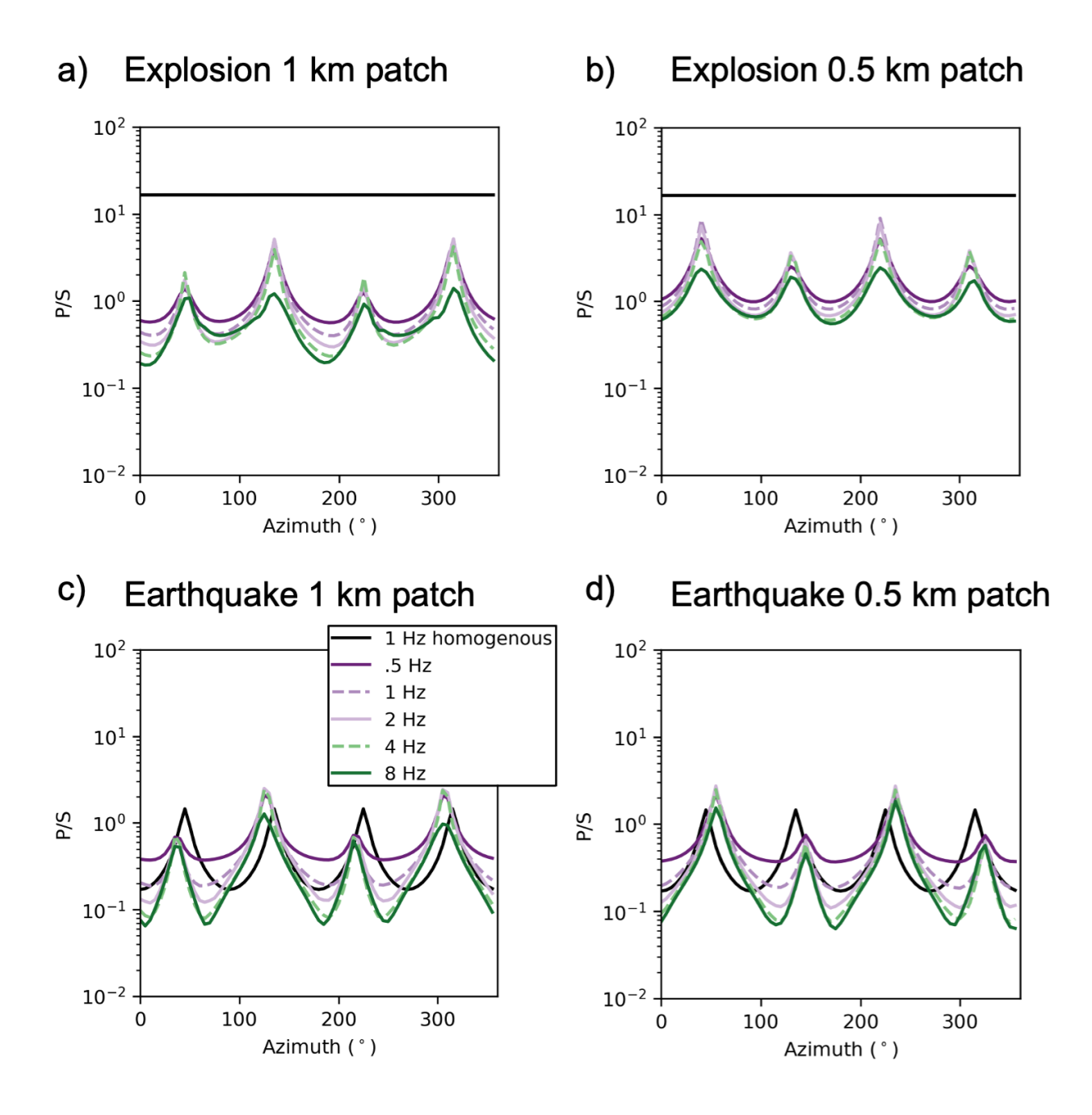


**Figure 7** Windowed P/S ratios for 2D synthetic seismograms plotted as a function of azimuth from the source for different source frequencies (0.5 Hz [dark purple], 1 Hz [dashed light purple], 2 Hz [solid light purple], 4 Hz [dashed light green], and 8 Hz [dark green]) and heterogeneous regional sizes (1 km vs 0.5 km) for explosion (a-b) and strike-slip earthquake sources (c-d). Each window is two seconds long with the arriving phase centered within the time window. In all scenarios, there is a region of small-scale heterogeneities except for the 1 Hz homogeneous case (black line). A 100 m-spaced mesh is applied in each of these scenarios. Figure S5 shows wavefield snapshots for these simulations.

# 3.4 3D Models of Small-Scale Heterogeneities

The observed long-period transverse component data can vary significantly compared to vertical and radial data from nearby nuclear tests at regional distances (1-20°) (e.g., Burgos et al., 2016). 3D simulations allow us to explore the effect that near-source small-scale heterogeneity has on the transverse component of seismograms and let us calculate the polarization angles for explosive events. An explosive event without near-source small-scale heterogeneities in a 1D flat-layer medium will always have a polarization angle of 0° (relative to the

back azimuth) as no SH energy is produced.

We use the SPECFEM3D-GLOBE (Komatitsch et al., 2010) software package to conduct 3D waveform simulations. We did not include the effects of topography, ellipticity, attenuation, or anisotropy in any of our 3D simulations. Including topography (Rodgers et al., 2010) or crustal anisotropy (Maupin, 1990) is expected to increase the amount of energy we observe on the transverse component. We placed surface stations in a circle at 5° azimuthal increments 400 km away from the source. The velocity model is the continental version of AK135 (Kennett et al., 1995). We tested both explosive

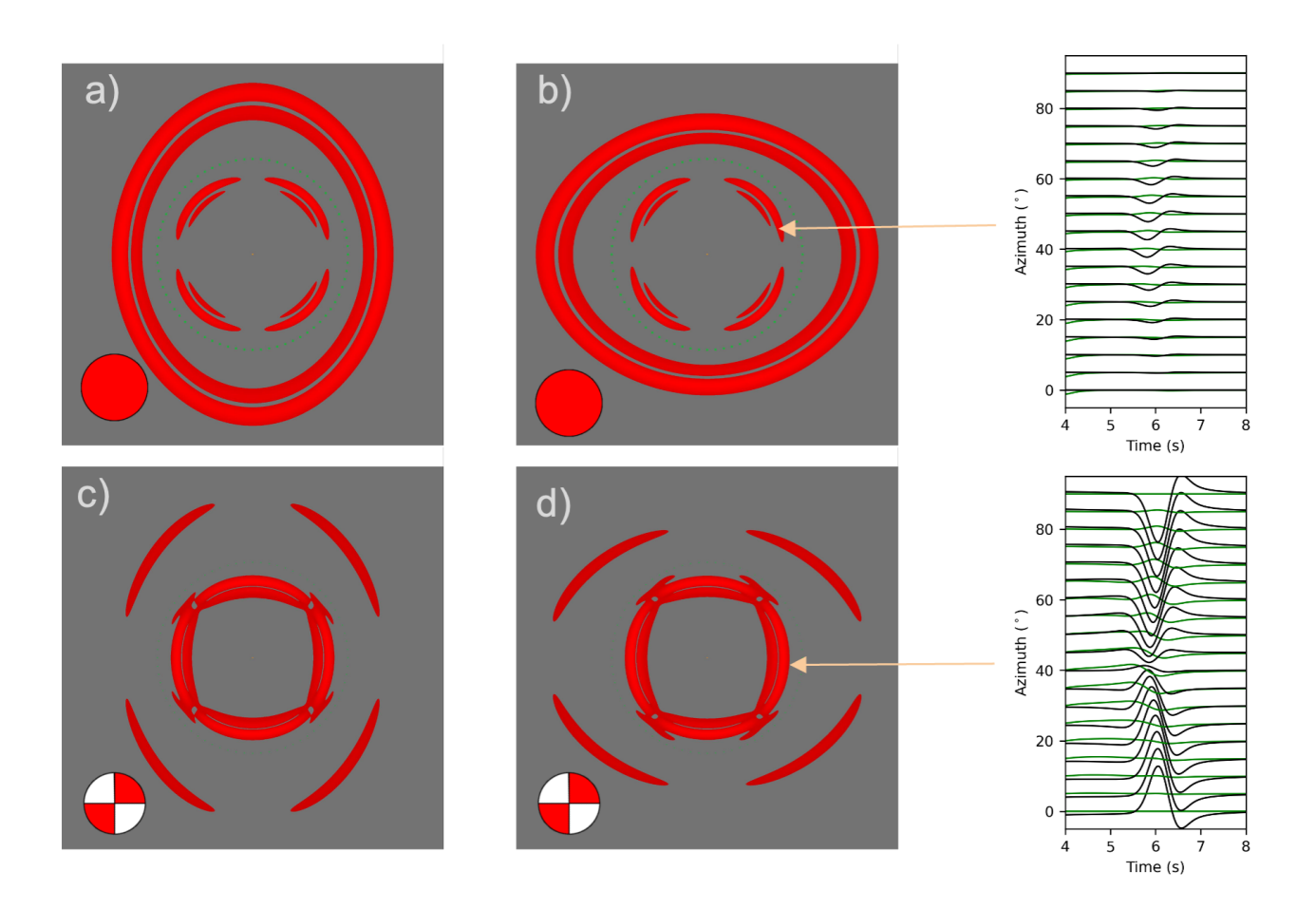


**Figure 8** 2D norm of displacement patterns and corresponding seismograms (azimuths ~0°-90°) of explosive and earth-quake sources within anisotropic media (fast direction alternates from horizontal to vertically fast directions) at 1 Hz: (a) explosive source with vertical fast direction, (b) explosive source with horizontally fast direction, (c) earthquake strike slip source with the same setup as (a), and (d) earthquake strike slip source with the same setup as (b). The source and receiver geometry is the same as Figure 2, and the entire domain is anisotropic. The seismograms illustrate the S-wave arrival for the radial (green lines) and transverse components (black lines) for the two VTI examples.

and earthquake sources with and without near-source heterogeneity with a half duration of 1.0 Hz. We model small-scale heterogeneities near the source as a 1 km  $\times$  1 km  $\times$  1 km cube with ± 25% random variations in Vp, Vs, and density. The source is located at the center of the heterogeneous region.

Figure 10 illustrates the results of our 3D simulations. The seismograms on the right show the effect of near source heterogeneity on the transverse component when we use an explosive source. As predicted, without heterogeneity the transverse component is zero (not shown in figure), but when we include it there is a clear but small-amplitude Sn arrival at 100 seconds which is followed by Lg and Love waves. The near-source heterogeneity does not significantly affect the vertical or radial component arrivals for a surface event but does convert some of the energy into the transverse component (see Supporting Figure S6).

The seismograms on the right also show an earthquake with near-source heterogeneities. Both source types produce clear arrivals; however, the explosive ones have much lower amplitudes on the transverse component and must be scaled by a factor of four to have comparable amplitudes to the earthquake. An interesting observation is how the Sn varies with azimuth. Even in this 60° azimuthal window, there are variations in peak amplitudes among the Sn arrivals for the earthquake while the peak amplitude of Sn for the explosion is constant. This is confirmed by measuring the P/S ratios and polarization angles. The top left of the figure shows P/S component energy ratios measuring the radial component (R) P and transverse component (T) S for different event types with and without near-source heterogeneity. We observe that the P/S ratio (or the R/T ratio) for the explosion with near-source heterogeneity is constant except at two distinct azimuths while both simulations for earthquakes show large changes over all azimuths.

The polarization measurements also show similar behavior. We measured the polarization angles as a function of azimuth for Sn using the time window indicated by magenta lines in the seismogram plots. The earth-quakes produce large variations in polarization angle as a function of azimuth. The homogenous measurements match predictions made for the corresponding moment tensor (Aki and Richards, 2002). Adding het-

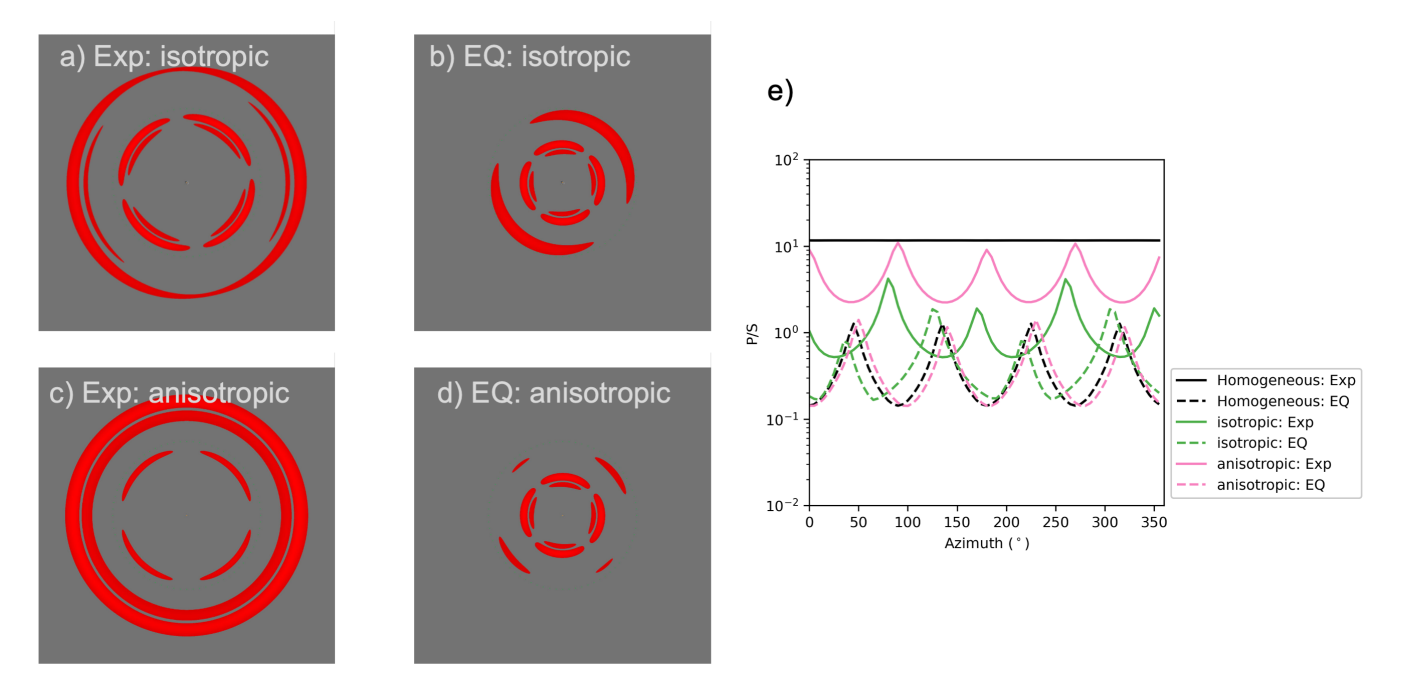


**Figure 9** 2D norm of displacement patterns and corresponding P/S ratios of explosive and earthquake sources with a 1 km-sized region with heterogeneous anisotropic media (HTI or VTI) at 1 Hz: (a) explosive source with 1 km isotropic heterogeneities, (b) earthquake source with 1 km isotropic heterogeneities, and (d) earthquake strike slip source with 1 km anisotropic heterogeneities. The source and receiver geometry is that of Figure 2. (e) P/S ratios for the various scenarios as a function of azimuth from the source. Black lines represent homogeneous simulation. All explosion results are displayed with solid lines, and earthquakes are displayed with dashed lines. Green lines correlate to (a) and (b) for isotropic heterogeneities, and pink lines correspond to (c) and (d) for anisotropic heterogeneities.

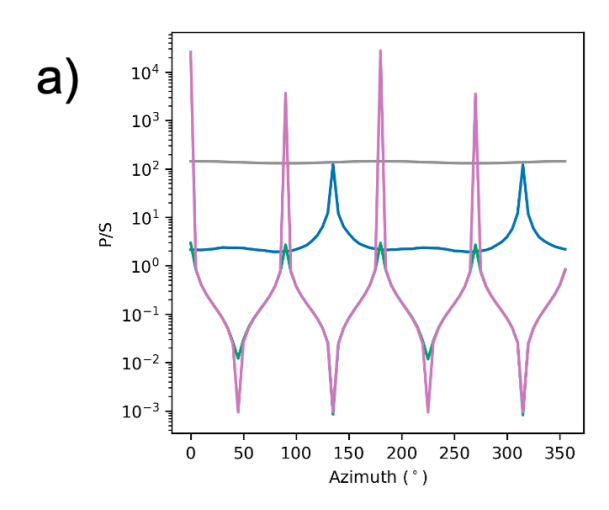
erogeneity near the earthquake source does not significantly affect the polarization angles, varying between ±10°. The apparent difference between 50°-100° is just an artifact of having values near 90°, where a minute difference can change the polarity from + or - 90°. For the homogenous explosion case, the polarization angle is, as expected, zero for all azimuths because there is no SH energy. When we include near source heterogeneity, there are small but non-zero polarization angles for most azimuths. The small P/S ratios can be explained by the small amplitudes of the Sn arrival on the transverse component compared to the radial component. However, transverse component energy can be increased by adding topography and/or anisotropy (Rodgers et al., 2010; Maupin, 1990). The polarization measurements also correlate with the P/S ratios (e.g., zero crossings of polarization angles correlate with high P/S ratios). As a result, including small-scale heterogeneity around the source cannot produce strong polarization angles as expected from earthquakes, whose polarization angles can vary significantly up to 90°. Further research is needed to evaluate if polarization angles of S-waves from explosions can help with discrimination.

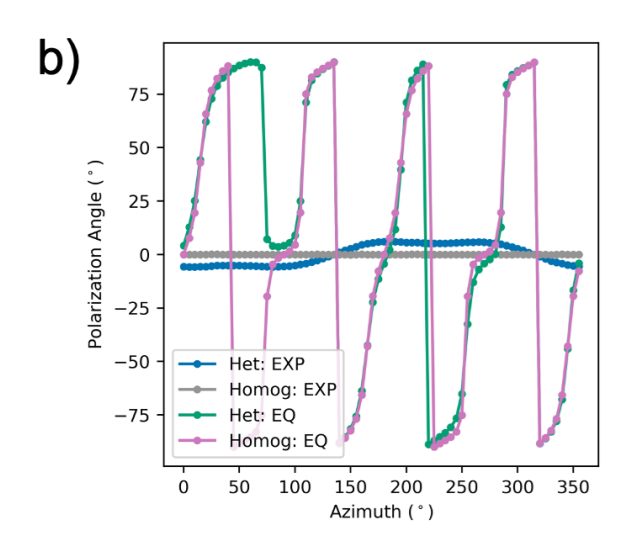
### 4 Discussion

Our work, along with the work of others such as Burgos et al. (2016), demonstrates that near-source elastic effects influence the resulting far-field radiation patterns from point sources. We show that this is true for both explosions and earthquakes. At certain az-

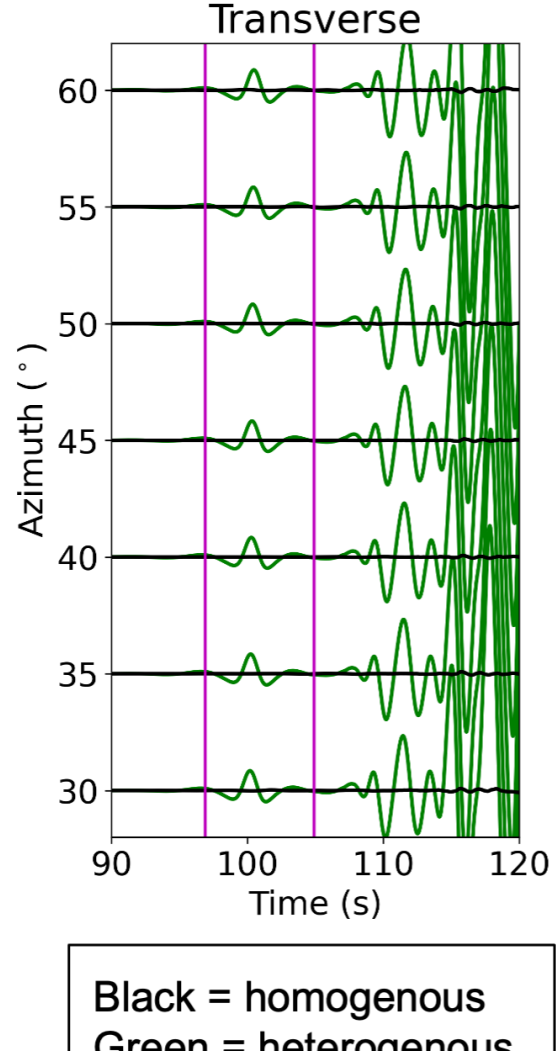
imuths, an explosive event in the presence of smallscale heterogeneity can produce an S-wavefield with an earthquake-like radiation pattern across all source frequencies we tested. We tested both a checkerboard arrangement of heterogeneities and a Gaussian distribution, showing that similar radiation patterns can be produced. In the presence of near-source small-scale heterogeneities, where only the shear moduli are changing (Supporting Figure S2), an explosive source in the elastic regime will produce an S-wavefield. Therefore, our observations agree with the following three predictions made by Leavy (1993) using first-order perturbation theory: the radiation pattern for S-waves 1) has a four-lobed pattern similar to an earthquake; 2) has the same frequency content as the P-wavefront originating at the source; and 3) is most strongly influenced by heterogeneities within subwavelength distances from the source and that subwavelength heterogeneities will become invisible to the wavefront farther away from the source.

The far-field of the point-source approximated earthquakes is also affected by near-source heterogeneities but not nearly on the same magnitude as explosions. The small-scale heterogeneities near the source region mainly impact the S-wavefield of explosions, while for earthquakes it is the P-wave field that mainly changes (Figure 3). Unlike explosions, all earthquakes rupture along a plane with finite dimensions. Earthquakes of magnitude less than 4.5 have rupture lengths of less than 1 km while earthquakes greater than 4.5 can have significantly longer rupture lengths, greater than 10 km





## c) Explosion Waveforms in 3D



Green = heterogenous

Figure 10 3D simulation results with SPECFEM3D\_GLOBE. (a) P/S component energy ratios for explosion with heterogeneities (red), explosion without (black), earthquake with heterogeneities (blue), and earthquake without (magenta). Solid lines represent P/SH (radial/transverse components) ratios, while dashed lines represent P/SV (radial/radial components). All P/SV ratios are quite similar and stack on top of each other. (b) Polarization measurements of synthetic waveforms. Color scheme is the same as (a). (c) Transverse component synthetic waveforms of explosion simulation with (green) and without (black) heterogeneities.

(Wells and Coppersmith, 1994). Therefore, it is likely that the source region encounters different near-field heterogeneities as the rupture propagates along the fault. With explosions, there is no large rupture, and the source is contained within a small volume (cavity sizes are on the order of ~1-100s of meters); therefore, there is no significant change in the source region properties. As a result, low magnitude earthquakes are very challenging to discriminate from nuclear or explosive tests because perhaps small earthquakes rupture over much shorter length scales that are comparable to the explosion cavity sizes. However, the main reason that discrimination can be challenging for low yield events is the limited data at near distances.

Burgos et al. (2016) compared long period (>30 s) ob-

servations from nearby nuclear tests carried out at the NNSS to stations at regional distances (<15 degrees). They found the stations often observed nearly identical radial and vertical component data but showed variations in their transverse components as a function of azimuth. In our 3D results, we also see nearly identical vertical and radial components (Figure S6), but the transverse components are different when adding small-scale heterogeneities, showing similar results to the NNSS tests. As a result, small-scale heterogeneities and/or anisotropy are plausible mechanisms to explain and better predict transverse component energy when using common earthquake and explosion discriminants, such as P/S ratios.

A unifying explanation which could possibly explain

why certain nearby explosive tests produce different S-wavefields while others fail to do so is the scale of shear modulus perturbations near the source. For SPE-2 and SPE-3, the damage done by SPE-2 to the nearby rock may have been insufficient to make a meaningful change to the rock's rigidity while Salmon experiment significantly changed the rigidity from around 3 GPa in the salt formation to 0 GPa in air. In the most general case, the aspherical geometry proposed by Xu et al. (2009), which explains the development of the S-wavefield in the Sterling test, can be treated as an extreme perturbation in seismic wave speeds and densities.

# 4.1 Earthquake and Explosion Discrimination with P/S Ratios

Small earthquakes can often occur in the same region as explosive tests (e.g., Taylor et al., 1989; Zeiler and Velasco, 2009). Therefore, distinguishing these types of sources is crucial in explosion monitoring and source identification and characterization. We also explore how these small-scale isotropic and anisotropic heterogeneities may influence seismic discrimination techniques. The main technique we analyze is P/S ratios.

When no small-scale heterogeneities or anisotropy are present, P/S ratios for explosive sources are predictably high and exhibit no azimuthal variation. For the strike-slip earthquake sources, the P/S ratios are also predictable in accordance with the source radiation pattern and are azimuthally varying, but there can be azimuths with little S-wave energy (see Figure 7). P/S ratios for earthquakes have a strong azimuthal pattern that will change with source type because of the changing radiation pattern. Based on our results with small-scale heterogeneities and explosive sources, P/S ratios have a strong dependence on source frequency, scale-length of small-scale heterogeneities, azimuth, and anisotropy. In the 2D cases, significant overlap can occur between the P/S ratios of the explosive and earthquake sources for certain azimuths, especially when Pwave energy is high for the earthquake source (see Figure 7). We do see P/S ratios reduce as the region of smallscale heterogeneities increases. Also, the generated Swave radiation pattern can resemble that of a strike-slip earthquake's S-wavefield. However, the exact wavefield of the explosive or earthquake sources will depend on the source mechanism, distributions of inhomogeneity, and the parameters of the power spectra, such as strength and correlation length.

In the case of anisotropy, all tests that included seismic anisotropy resulted in S-wave generation from an explosive source. The resulting S-wavefield (Figures 8 and 9) also produces radiation patterns akin to an earthquake. The Earth is anisotropic, especially in Earth's crust, which would make the scenarios plausible. Most crustal rocks have hexagonal symmetry (biotite and olivine), which we tested here in 2D (Brownlee et al., 2017). Some crustal minerals, such as quartz and plagioclase, exhibit lower-order symmetries, which are being investigated in a future study. Anisotropy requires 3D and should be tested within that space, especially to explore lower symmetries of orthorhombic and tri-

clinic symmetries. In these experiments, we tested 20% anisotropy, which is within reasonable crustal rock anisotropies (~5-20%) measured in regions of high shear strain (e.g., Brownlee et al., 2017; Tatham et al., 2008). However, single-crystal seismic anisotropy measurements can be as high as 43%, 34%, 31%, and over 50% Vs anisotropy for quartz, plagioclase, hornblende, and micas, respectively (Brownlee et al., 2017; Tatham et al., 2008; McSkimin et al., 1965; Vaughan and Guggenheim, 1986). Therefore, either anisotropy or small-scale heterogeneity (isotropic or anisotropic) can produce lower P/S ratios. At certain azimuths, P/S ratios cannot distinguish between explosions and earthquakes, like what Zhang (2023) illustrated.

# 4.2 Observations and application to explosion monitoring

As a result of this study, we identify reasons why P/S ratios are not always a reliable metric for discriminating between small, shallow earthquakes and explosions. Usually, other metrics are analyzed in combination with P/S ratios to fully differentiate events, such as infrasound and radionuclide monitoring (e.g., Bowers and Selby, 2009; Coyne et al., 2012). In the presence of smallscale heterogeneities or anisotropy, P/S ratios will be less reliable. In all tests, S-waves were generated in the presence of near-source heterogeneity, and the radiation pattern could significantly differ depending on the parameters of the small-scale heterogeneities. The resulting radiation pattern for explosions is highly sensitive to the source location (Figure 4), source frequency (Figure 7), and scale of heterogeneities (Figure 5); therefore, it may be difficult to simulate the same S-wave radiation pattern of real explosive sources in heterogeneous media. For earthquakes, however, the radiation pattern mostly stays the same (Figures 8 and 9) even in the presence of anisotropy.

One other discriminant method we explored is the azimuthal dependence of S-wave polarizations with a 3D simulation, which is related to the ratio of SV to SH energy. We find that earthquake source polarizations do not significantly change in the presence of small-scale heterogeneities. An explosive source in the presence of small-scale heterogeneities produced some SH energy, but it was still small relative to the SV energy, resulting in small S-wave polarizations (Figure 10); and its radiation pattern is not very similar to a possible earthquake, as the SV energy is much more significant than any produced SH energy. A more complex and realistic 3D Earth model which includes anisotropy or topography will produce significantly more SH energy than what we observed (Maupin, 1990; Rodgers et al., 2010). However, a much more rigorous investigation that is beyond the scope of this study comparing observations to synthetically generated waveforms is required to quantify their effects.

Lastly, modeling small-scale heterogeneity is computationally expensive, where other methods are needed, such as homogenization of the source model to the source model or envelope modeling (Mancinelli et al., 2016). Significant research has been conducted in

this area in application to earthquakes (e.g., Capdeville et al., 2020; Capdeville, 2021) and explosions (e.g., Burgos et al., 2016). While implementing homogenization techniques is not the focus of this study, homogenization methods could be used in the future in applications to explosion discrimination techniques, such as P/S ratios to reduce computational costs of simulations. Additionally, effective medium theory is another application for avoiding the high computational cost, while also capturing the complexity of small-scale heterogeneities (e.g., Jordan, 2015; Hudson, 1980; Backus, 1962). Effective medium theory is like homogenization, but instead of altering the source or wave equation itself, an effective elastic tensor is calculated to represent the isotropic heterogeneities that are significantly smaller than the effective wavelength, such as small cracks, polycrystalline aggregates, disordered lithologic units, etc. Many of the wavefield observations in our study (such as Figures 3b-3c) could be reproduced with effective medium theory. The heterogeneities can be modeled as spheroids, cracks, thin horizontal layers, ellipsoids, and similar features. Using effective medium theory and the influence on P/S ratios is of potential interest for future research.

## 5 Conclusions

In this study, we illustrate how explosion/earthquake discriminants (such as P/S ratios) have significant azimuthal variations in the presence of isotropic or anisotropic small-scale heterogeneities within the source region. Based on our 2D results, the P/S ratios are nearly indistinguishable between earthquakes and explosions, where for both sources the P/S ratios are on the scale of 10<sup>-1</sup> to 10<sup>0</sup>. We find for our simulation setups that if the region of scatterers is on the order of 1/12 compared to the S-wavelength, then an S-wavefield is produced. However, in the 3D case, small-scale heterogeneities also decrease P/S ratios for explosive sources, but not as significantly as the 2D case. There was no significant SH energy for the first arriving S-wave, which diverges from observations of some explosive sources. Energy on the transverse component was very small, resulting in a P/S ratio for the explosive sources in the range from  $10^{0}$ – $10^{2}$ . For the earthquakes, P/S ratios were  $\sim 10^{-2}-10^{1}$ . Notably, we only considered strike-slip events for the earthquakes. For other moment tensors, P/S ratios will slightly vary azimuthally.

To summarize, we show that small-scale heterogeneities (isotropic or anisotropic) near a source modify both P and S-wave radiation patterns for explosions and strike-slip earthquakes. When no small-scale heterogeneities or anisotropy are present for explosive sources, then P/S ratios are predictably high and have no azimuthal variation. For earthquake sources, the P/S ratios are also predictable in accordance with the source and are azimuthally varying. Source frequency has a modest effect on P/S ratios, especially as the size of the near-source heterogeneity decreases. With high source frequencies and explosive sources, P/S ratios decrease and show much more uniform azimuthal pattern. The larger the region of the near-source heterogeneities, the

lower the P/S ratios of explosive sources, until a certain threshold is reached. Small-scale heterogeneities that are anisotropic can also produce S-waves from explosive sources. P/S ratios are highly dependent on azimuth, where certain azimuths may be extremely difficult to differentiate explosions and earthquakes. To improve source discrimination, additional data analysis will be required, such as azimuthally varying data collection, numerical simulations, source-depth constraints, constraints on scatterer density and location, and other discrimination methods should be used in combination with P/S ratios.

## **Acknowledgements**

Thoughtful and constructive discussions with Scott Phillips, Eli Baker, Mike Begnaud, Cathy Snelson, Kai Gao, Ryan Modrak, Howard Patton, and Garret Euler improved this manuscript. This research used resources provided by the Los Alamos National Laboratory Institutional Computing Program, which is supported by the U.S. Department of Energy National Nuclear Security Administration under Contract No. 89233218CNA000001. This Ground-based Nuclear Detonation Detection (GNDD) research was funded by the National Nuclear Security Administration, Defense Nuclear Nonproliferation Research and Development (NNSA DNN R&D). High-performance computing resources were provided by the LANL Institutional Computing Program. This work is released under LA-UR-23-30729. We also thank Carl Tape and three anonymous reviewers for their valuable feedback. We thank the Computational Infrastructure for Geodynamics (http:// geodynamics.org) which is funded by the National Science Foundation under awards EAR-0949446, 1550901 and 2149126.

## Data and code availability

SPECFEM input files are available in the supporting information found in a Mendeley repository (Nelson and Creasy, 2025). No data was used in this study. We use SPECFEM2D v7.0 and SPECFEM3D\_GLOBE v7.0.02 (Tromp et al., 2008; Komatitsch and Tromp, 2002a,b) published under the GPL 3 licenses.

## **Competing interests**

The authors have no competing interests.

## References

Aki, K. and Richards, P. Quantitative seismology. 2002.

Aki, K., Reasenberg, P., DeFazio, T., and Tsai, Y. Near-field and far-field seismic evidences for triggering of an earthquake by the Benham explosion. *Bulletin of the Seismological Society of America*, 59(6):2197–2207, 1969.

Anderson, D. L. Elastic wave propagation in layered anisotropic media. *Journal of Geophysical Research*, 66(9):2953–2963, Sept. 1961. doi: 10.1029/jz066i009p02953.

- Backus, G. Long-wave elastic anisotropy produced by horizontal layering. *Journal of Geophysical Research*, 67(11), 1962. doi: 10.1002/2015JB012641.
- Baker, G. E., Stevens, J. L., and Xu, H. Explosion Shear-Wave Generation in High-Velocity Source Media. *Bulletin of the Seismological Society of America*, 102(4):1301–1319, Aug. 2012. doi: 10.1785/0120110119.
- Ben-Menahem, A., Gibson Jr, R. L., and Sena, A. G. Green's tensor and radiation patterns of point sources in general anisotropic inhomogeneous elastic media. *Geophysical journal international*, 107(2), 1991. doi: 10.1111/j.1365-246X.1991.tb00827.x.
- Ben-Menahem, A. and Sena, A. G. Seismic source theory in stratified anisotropic media. *Journal of Geophysical Research: Solid Earth*, 95(B10):15395–15427, Sept. 1990. doi: 10.1029/jb095ib10p15395.
- Blandford, R. R. *Seismic Discrimination Problems at Regional Distances*, page 695–740. Springer Netherlands, 1981. doi: 10.1007/978-94-009-8531-5\_38.
- Bowers, D. and Selby, N. D. Forensic Seismology and the Comprehensive Nuclear-Test-Ban Treaty. *Annual Review of Earth and Planetary Sciences*, 37(1):209–236, May 2009. doi: 10.1146/annurev.earth.36.031207.124143.
- Brownlee, S. J., Schulte-Pelkum, V., Raju, A., Mahan, K., Condit, C., and Orlandini, O. F. Characteristics of deep crustal seismic anisotropy from a compilation of rock elasticity tensors and their expression in receiver functions. *Tectonics*, 36(9): 1835–1857, Sept. 2017. doi: 10.1002/2017tc004625.
- Brune, J. N. and Pomeroy, P. W. Surface wave radiation patterns for underground nuclear explosions and small-magnitude earth-quakes. *Journal of Geophysical Research*, 68(17):5005–5028, Sept. 1963. doi: 10.1029/jz068i017p05005.
- Burgos, G., Capdeville, Y., and Guillot, L. Homogenized moment tensor and the effect of near-field heterogeneities on non-isotropic radiation in nuclear explosion. *Journal of Geophysical Research: Solid Earth*, 121(6):4366–4389, June 2016. doi: 10.1002/2015jb012744.
- Capdeville, Y. Homogenization of seismic point and extended sources. *Geophysical Journal International*, 226(2):1390–1416, May 2021. doi: 10.1093/gji/ggab178.
- Capdeville, Y., Guillot, L., and Marigo, J.-J. 2-D non-periodic homogenization to upscale elastic media for P–SV waves. *Geophysical Journal International*, 182(2):903–922, June 2010. doi: 10.1111/j.1365-246x.2010.04636.x.
- Capdeville, Y., Cupillard, P., and Singh, S. An introduction to the two-scale homogenization method for seismology. In *Advances in Geophysics*, volume 61, page 217–306. Elsevier., DOI, 2020. 10.1016/bs.agph.2020.07.001.
- Coyne, J., Bobrov, D., Bormann, P., Duran, E., Grenard, P., Haralabus, G., Kitov, I., and Starovoit, Y. CTBTO: Goals, networks, data analysis and data availability. In *New manual of seismological observatory practice 2 (NMSOP-2)*. Deutsches GeoForschungsZentrum GFZ, 2012. doi: 10.2312/GFZ.NMSOP-2\_ch15.
- Denny, M. D. and Goodman, D. M. A case study of the seismic source function: Salmon and sterling reevaluated. *Journal of Geophysical Research: Solid Earth*, 95(B12):19705–19723, Nov. 1990. doi: 10.1029/jb095ib12p19705.
- Ekström, G. and Richards, P. G. Empirical Measurements of Tectonic Moment Release In Nuclear Explosions From Teleseismic Surface Waves and Body Waves. *Geophysical Journal International*, 117(1):120–140, Apr. 1994. doi: 10.1111/j.1365-246x.1994.tb03307.x.
- Gajewski, D. Radiation from point sources in general anisotropic

- media. *Geophysical Journal International*, 113(2):299–317, May 1993. doi: 10.1111/j.1365-246x.1993.tb00889.x.
- Gualtieri, L., Stutzmann, E., Juretzek, C., Hadziioannou, C., and Ardhuin, F. Global scale analysis and modelling of primary microseisms. *Geophysical Journal International*, 218(1):560–572, Mar. 2019. doi: 10.1093/gji/ggz161.
- Gupta, I., Chan, W., and Wagner, R. A comparison of regional phases from underground nuclear explosions at east Kazakh and Nevada test sites. *Bulletin of the Seismological Society of America*, 82(1):352–382, 1992.
- Hartse, H. E., Taylor, S. R., Phillips, W. S., and Randall, G. E. A preliminary study of regional seismic discrimination in central Asia with emphasis on western China. *Bulletin of the Seismological Society of America*, 87(3):551–568, June 1997. doi: 10.1785/b-ssa0870030551.
- Healy, J. H., King, C.-Y., and O'Neill, M. E. Source parameters of the Salmon and Sterling Nuclear Explosions from seismic measurements. *Journal of Geophysical Research*, 76(14):3344–3355, May 1971. doi: 10.1029/jb076i014p03344.
- Hirakawa, E., Pitarka, A., and Mellors, R. Generation of Shear Motion from an Isotropic Explosion Source by Scattering in Heterogeneous Media. *Bulletin of the Seismological Society of America*, 106(5):2313–2319, July 2016. doi: 10.1785/0120150243.
- Houng, S. E. Discrimination between Natural Earthquakes and Explosions Based on the Azimuthal Distribution of S/P Amplitude Ratios. *Bulletin of the Seismological Society of America*, 108(1): 218–229, Dec. 2017. doi: 10.1785/0120160322.
- Hudson, J. Overall properties of a cracked solid. *Mathematical Proceedings of the Cambridge Philosophical Society*, 88(2), 1980. doi: 10.1017/S0305004100057674.
- Jenkins, R. and Sereno, Jr, T. Calibration of regional S/P amplitude-ratio discriminants. *pure and applied geophysics*, 158:1279–1300, 2001.
- Jordan, T. An effective medium theory for three-dimensional elastic heterogeneities. *Geophysical Journal International*, 203(2), 2015. doi: 10.1093/gji/ggv355.
- Kennett, B. L. N., Engdahl, E. R., and Buland, R. Constraints on seismic velocities in the Earth from traveltimes. *Geophysical Journal International*, 122(1):108–124, July 1995. doi: 10.1111/j.1365-246x.1995.tb03540.x.
- Komatitsch, D. and Tromp, J. Spectral-element simulations of global seismic wave propagation-I. Validation. *Geophysical Journal International*, 149(2):390–412, May 2002a. doi: 10.1046/j.1365-246x.2002.01653.x.
- Komatitsch, D. and Tromp, J. Spectral-element simulations of global seismic wave propagation-II. Three-dimensional models, oceans, rotation and self-gravitation. *Geophysical Journal International*, 150(1):303–318, July 2002b. doi: 10.1046/j.1365-246x.2002.01716.x.
- Komatitsch, D. and Vilotte, J.-P. The spectral element method: An efficient tool to simulate the seismic response of 2D and 3D geological structures. *Bulletin of the Seismological Society of America*, 88(2):368–392, Apr. 1998. doi: 10.1785/bssa0880020368.
- Komatitsch, D., Erlebacher, G., Göddeke, D., and Michéa, D. Highorder finite-element seismic wave propagation modeling with MPI on a large GPU cluster. *Journal of Computational Physics*, 229(20):7692–7714, Oct. 2010. doi: 10.1016/j.jcp.2010.06.024.
- Leavy, D. Scattering of elastic waves near an explosion. *Bulletin of the Seismological Society of America*, 83(4):1277–1293, Aug. 1993. doi: 10.1785/bssa0830041277.
- Leng, K., Korenaga, J., and Nissen-Meyer, T. 3-D scattering of elastic waves by small-scale heterogeneities in the Earth's mantle. *Geophysical Journal International*, 223(1):502–525, July 2020.

- doi: 10.1093/gji/ggaa331.
- Li, H., Qu, K., Rong, W., Tuo, X., Lu, J., Wang, R., Wang, X., and Courtois, J. PolarGUI: A MATLAB-Based Tool for Polarization Analysis of the Three-Component Seismic Data Using Different Algorithms. *Seismological Research Letters*, 92(6):3821–3831, July 2021. doi: 10.1785/0220200439.
- Mancinelli, N., Shearer, P., and Liu, Q. Constraints on the heterogeneity spectrum of Earth's upper mantle. *Journal of Geophysical Research: Solid Earth*, 121(5), 2016. doi: 10.1002/2015JB012641.
- Mandal, B. and Toksöz, M. N. Computation of complete waveforms in general anisotropic media-results from an explosion source in an anisotropic medium. *Geophysical Journal International*, 103(1):33–45, Oct. 1990. doi: 10.1111/j.1365-246x.1990.tb01750.x.
- Martynov, V. N. and Mikhailenko, B. G. Numerical modelling of propagation of elastic waves in anisotropic inhomogeneous media for the half-space and the sphere. *Geophysical Journal International*, 76(1):53–63, Jan. 1984. doi: 10.1111/j.1365-246x.1984.tb05021.x.
- Maupin, V. Modeling of three-component Lg waves in anisotropic crustal models. *Bulletin of the Seismological Society of America*, 80(5):1311–1325, 1990.
- McSkimin, H. J., Andreatch, P., and Thurston, R. N. Elastic Moduli of Quartz versus Hydrostatic Pressure at 25° and 195.8°C. *Journal of Applied Physics*, 36(5):1624–1632, May 1965. doi: 10.1063/1.1703099.
- Mellors, R., Myers, S., Ford, S., Walter, W., Hauk, T., Ruppert, S., and Pitarka, A. SPE3 Far-field Quicklook. Technical Report LLNL-TR-586676, Office of Scientific and Technical Information (OSTI), Lawrence Livermore National Laboratory, Sept. 2012. doi: 10.2172/1053657.
- Moschetti, M. P., Ritzwoller, M. H., Lin, F., and Yang, Y. Seismic evidence for widespread western-US deep-crustal deformation caused by extension. *Nature*, 464(7290):885–889, Apr. 2010. doi: 10.1038/nature08951.
- Myers, S. C., Walter, W. R., Mayeda, K., and Glenn, L. Observations in support of Rg scattering as a source for explosion S waves: Regional and local recordings of the 1997 Kazakhstan depth of burial experiment. *Bulletin of the Seismological Society of America*, 89(2):544–549, Apr. 1999. doi: 10.1785/bssa0890020544.
- Mykkeltveit, S. and Husebye, E. S. *Lg Wave Propagation in Eurasia*, page 421–451. Springer Netherlands, 1981. doi: 10.1007/978-94-009-8531-5 21.
- Nelson, P. and Creasy, N. Shear-Wave Radiation Patterns from Explosive and Earthquaker Sources in Scattering, Heterogeneous Media [dataset]. Mendeley Data, 2025. doi: 10.17632/54kkx44886.2.
- Nelson, P. L., Modrak, R. T., Phillips, W. S., and Begnaud, M. Finite-Frequency Kernels for Pg Wavetrains. *Bulletin of the Seismological Society of America*, 113(3):1039–1053, Feb. 2023. doi: 10.1785/0120220162.
- Nuttli, O. W. Lg magnitudes of selected East Kazakhstan underground explosions. *Bulletin of the Seismological Society of America*, 76(5):1241–1251, Oct. 1986. doi: 10.1785/bssa0760051241.
- O'Rourke, C. T., Baker, G. E., and Sheehan, A. F. Using P/S amplitude ratios for seismic discrimination at local distances. *Bulletin of the Seismological Society of America*, 106(5):2320–2331, July 2016. doi: 10.1785/0120160035.
- Patton, H. J. Seismic moment estimation and the scaling of the longperiod explosion source spectrum, page 171–183. American Geophysical Union, 1991. doi: 10.1029/gm065p0171.
- Perret, W. R. Shear waves from a nuclear explosion in a salt

- cavity. Bulletin of the Seismological Society of America, 58(6): 2043–2051, Dec. 1968. doi: 10.1785/bssa0580062043.
- Peter, D., Komatitsch, D., Luo, Y., Martin, R., Le Goff, N., Casarotti, E., Le Loher, P., Magnoni, F., Liu, Q., Blitz, C., Nissen-Meyer, T., Basini, P., and Tromp, J. Forward and adjoint simulations of seismic wave propagation on fully unstructured hexahedral meshes: SPECFEM3D Version 2.0 'Sesame'. *Geophysical Journal International*, 186(2):721–739, May 2011. doi: 10.1111/j.1365-246x.2011.05044.x.
- Pienkowska, M., Monteiller, V., and Nissen-Meyer, T. High-frequency global wavefields for local 3-D structures by wavefield injection and extrapolation. *Geophysical Journal International*, 225(3):1782–1798, Nov. 2020. doi: 10.1093/gji/ggaa563.
- Press, F. and Archambeau, C. Release of tectonic strain by underground nuclear explosions. *Journal of Geophysical Research*, 67 (1):337–343, Jan. 1962. doi: 10.1029/jz067i001p00337.
- Priestley, K. F., Walter, W. R., Martynov, V., and Rozhkov, M. V. Regional seismic recordings of the Soviet nuclear explosion of the Joint Verification Experiment. *Geophysical Research Letters*, 17 (2):179–182, Feb. 1990. doi: 10.1029/gl017i002p00179.
- Richards, P. G. and Kim, W.-Y. Testing the nuclear test-ban treaty. *Nature*, 389(6653):781–782, Oct. 1997. doi: 10.1038/39720.
- Richards, P. G. and Zavales, J. SEISMIC DISCRIMINATION OF NUCLEAR EXPLOSIONS. *Annual Review of Earth and Planetary Sciences*, 18(1):257–286, May 1990. doi: 10.1146/annurev.ea.18.050190.001353.
- Rodgers, A. J., Petersson, N. A., and Sjogreen, B. Simulation of topographic effects on seismic waves from shallow explosions near the North Korean nuclear test site with emphasis on shear wave generation. *Journal of Geophysical Research: Solid Earth*, 115(B11), Nov. 2010. doi: 10.1029/2010jb007707.
- Sato, H. Retrieval of Green's function having coda from the cross-correlation function in a scattering medium illuminated by surrounding noise sources on the basis of the first order Born approximation. *Geophysical Journal International*, 179(1), 2009. doi: 10.1111/j.1365-246X.2009.04296.x.
- Sato, H., Fehler, M. C., and Maeda, T. *Seismic wave propagation and scattering in the heterogeneous earth.* Springer Berlin Heidelberg, 2012. doi: 10.1007/978-3-642-23029-5.
- Savage, M. K. Seismic anisotropy and mantle deformation: What have we learned from shear wave splitting? *Reviews of Geophysics*, 37(1):65–106, Feb. 1999. doi: 10.1029/98rg02075.
- Silver, P. G. and Chan, W. W. Shear wave splitting and subcontinental mantle deformation. *Journal of Geophysical Research: Solid Earth*, 96(B10):16429–16454, Sept. 1991. doi: 10.1029/91jb00899.
- Singh, S. and Herrmann, R. B. Regionalization of crustal coda Q in the continental United States. *Journal of Geophysical Research: Solid Earth*, 88(B1):527–538, Jan. 1983. doi: 10.1029/jb088ib01p00527.
- Snelson, C. M., Abbott, R. E., Broome, S. T., Mellors, R. J., Patton, H. J., Sussman, A. J., Townsend, M. J., and Walter, W. R. Chemical Explosion Experiments to Improve Nuclear Test Monitoring. *Eos, Transactions American Geophysical Union*, 94(27):237–239, July 2013. doi: 10.1002/2013eo270002.
- Stroujkova, A., Bonner, J. L., Leidig, M., Boyd, P., and Martin, R. J. Shear Waves from Explosions in Granite Revisited: Lessons Learned from the New England Damage Experiment. *Bulletin of the Seismological Society of America*, 102(5):1913–1926, Oct. 2012. doi: 10.1785/0120110204.
- Tatham, D., Lloyd, G., Butler, R., and Casey, M. Amphibole and lower crustal seismic properties. *Earth and Planetary Science Letters*, 267(1–2):118–128, Mar. 2008. doi:

- 10.1016/j.epsl.2007.11.042.
- Taylor, S. R., Denny, M. D., Vergino, E. S., and Glaser, R. E. Regional discrimination between NTS explosions and western U.S. earthquakes. *Bulletin of the Seismological Society of America*, 79(4): 1142–1176, Aug. 1989. doi: 10.1785/bssa0790041142.
- Tromp, J., Komatitsch, D., and Liu, Q. Spectral-element and adjoint methods in seismology. *Communications in Computational Physics*, 3(1):1–32, 2008.
- Vaughan, M. T. and Guggenheim, S. Elasticity of muscovite and its relationship to crystal structure. *Journal of Geophysical Research: Solid Earth*, 91(B5):4657–4664, Apr. 1986. doi: 10.1029/jb091ib05p04657.
- Vavryčuk, V. and Kim, S. G. Nonisotropic radiation of the 2013 North Korean nuclear explosion. *Geophysical Research Letters*, 41(20):7048–7056, Oct. 2014. doi: 10.1002/2014gl061265.
- Vorobiev, O. On various mechanisms of shear wave generation from underground chemical explosions in hard rocks. *Geophysical Journal International*, 232(3):2133–2159, Nov. 2022. doi: 10.1093/gji/ggac442.
- Walker, A. M. and Wookey, J. MSAT—A new toolkit for the analysis of elastic and seismic anisotropy. *Computers & Geosciences*, 49: 81–90, Dec. 2012. doi: 10.1016/j.cageo.2012.05.031.
- Walter, W. R., Dodge, D. A., Ichinose, G., Myers, S. C., Pasyanos, M. E., and Ford, S. R. Body-Wave Methods of Distinguishing between Explosions, Collapses, and Earthquakes: Application to Recent Events in North Korea. *Seismological Research Letters*, Sept. 2018. doi: 10.1785/0220180128.
- Wang, R., Schmandt, B., and Kiser, E. Seismic Discrimination of Controlled Explosions and Earthquakes Near Mount St. Helens Using P/S Ratios. *Journal of Geophysical Research: Solid Earth*, 125(10), Sept. 2020. doi: 10.1029/2020jb020338.
- Wells, D. L. and Coppersmith, K. J. New empirical relationships among magnitude, rupture length, rupture width, rupture area, and surface displacement. *Bulletin of the Seismological Society of America*, 84(4):974–1002, Aug. 1994. doi: 10.1785/b-ssa0840040974.
- Xie, J. and Patton, H. J. Regional phase excitation and propagation in the Lop Nor region of central Asia and implications for P/Lg discriminants. *Journal of Geophysical Research: Solid Earth*, 104 (B1):941–954, Jan. 1999. doi: 10.1029/1998jb900045.
- Xie, Z., Komatitsch, D., Martin, R., and Matzen, R. Improved forward wave propagation and adjoint-based sensitivity kernel calculations using a numerically stable finite-element PML. *Geophysical Journal International*, 198(3):1714–1747, July 2014. doi: 10.1093/gji/ggu219.
- Xu, H., Stevens, J. L., and Baker, G. E. An analysis of shear waves generated by the Sterling explosion. *Journal of Geophysical Research: Solid Earth*, 114(B3), Mar. 2009. doi: 10.1029/2008jb005966.
- Zeiler, C. and Velasco, A. A. Developing Local to Near-Regional Explosion and Earthquake Discriminants. *Bulletin of the Seismological Society of America*, 99(1):24–35, Feb. 2009. doi: 10.1785/0120080045.
- Zhang, M. P/SV Amplitude Ratios of Shallow Isotropic Explosions and Earthquakes Could Be Indistinguishable at Local Distances: Insights from Single-Station Waveform Simulations. *The Seismic Record*, 3(1):48–56, Jan. 2023. doi: 10.1785/0320220044.

The article Shear-Wave Radiation Patterns from Explosive and Earthquake Sources in Scattering, Heterogeneous Media © 2025 by Peter Nelson is licensed under CC BY 4.0.